Data geometric supervised learning

Anonymous Author 1
Unknown Institution 1

Anonymous Author 2
Unknown Institution 2

Anonymous Author 3
Unknown Institution 3

Abstract

We develop a method for tracing out the shape of a cloud of sample observations, in arbitrary dimensions, called the *data cloud wrapper* (DCW). This is based on a recently developed *projection quantiles* (PQ) for multivariate random variables. The DCW have strong theoretical properties, have algorithmic scalability and parallel computational features. We then develop a notion of *data-depth* based on the DCW, which quantifies how deep a point in space or an observation lies with respect to the data geometry. We further use the DCW to develop a new fast and accurate classification method in high dimensions, called the **geometric learning algorithm**. Two of the main features of the proposed algorithm are that there are no assumptions made about the geometric properties of the underlying data generating distribution (hence the name), and that there are no parametric or other restrictive assumptions made either for the data or the algorithm. The proposed methods are competitive or better than several established classification techniques, when compared in terms of classification accuracy, speed of computation, or breadth of applicability.

1 Introduction

We propose a new method for supervised learning, or classification, that respects the inherent geometry of the data cloud for each labeled group of observations, and this method is not subject to curse of dimensionality. Our method is based on *multivariate quantiles*, which generalize the notion of quantiles for observations in dimensions greater than one. Arising naturally from the concept of multivariate quantiles is the notion of *data depth*, which is a relative measure of proximity of a given point in space to a collection of observations. For any new or unlabeled observation in the feature space, we estimate the label by computing its depth from the data clouds corresponding to a training data.

There are two important properties of the supervised learning technique presented below. First, we do not make assumptions about the shape of the different data clouds corresponding to various labels in the training sample. The proposed method respects the geometric properties of the data, and does not impose shape restrictions on it, hence we call it *geometric learning* algorithm. Second, our method is scalable and parallelizable with respect to dimensions and sample size, and does not suffer from the curse of dimensionality, and hence is extremely fast in implementation.

The strengths of the proposed geometric learning method arises from the fact that it is based on multivariate quantiles. In Section 2 we discuss these quantiles in details. Based on projection quantiles, which are a form of multivariate quantiles, we develop a *Data Cloud Wrap* (DCW) procedure that provides a very accurate description of the geometry of any sized data set in any dimension. As an illustration, consider Figure 1, which contains two bivariate scatter plots, the left panel being that of observations from a Gaussian distribution and the right panel is where observations are from a mixture of two Gaussian distributions. The red curves are obtained by the DCW procedure, and it can be seen that these curves quite accurately capture the geometry of the layout of the observations in either panel. The blue curves in either panel correspond to a PQ, which reasonably trace the shapes of the data clouds, but not as accurately as the DCW curves.

Preliminary work. Under review by AISTATS 2015. Do not distribute.

The black curves are obtained by presuming a Gaussian distribution for the data, with only mean and functions as unknowns. Notice that while this is adequate for capturing the shape of the data cloud when the Gaussian assumption holds, it is a severe misfit when the assumption is violated. The regions enclosed by the different curves in either panel are not expected to have have identical probabilistic coverage, owing to different mathematical properties.

Note that in high dimensions, it is essentially impossible to graphically or otherwise elicit how and where assumptions like Gaussian shape of the data geometry are violated. Even if such elicitation were feasible, it is unclear how to use that information for supervised learning, or other data-related tasks. The *geometric learning algorithm* we present here is a clear alternative, that does not rely on such encumbering assumptions.

We discuss below how the sets of Figure 1, and their enclosing boundary curves, may be indexed by vectors of the unit sphere in the feature space. Curves and enclosed sets as in Figure 1 are fast and accurate visualization tools that are easily available from the proposed procedure. These graphical techniques are naturally best suited for two and three dimensional projections of the data, however, the construction of such sets in any dimension is simple and quick in our proposed methodology. We can take full advantage of distributed and parallel computing tools for this purpose, since the constructions of sets like the ones depicted in Figure 1 is linear in both dimension (p) of the feature space, and the number of observations (n), and parallelizable in both dimensions and sample size. Since the DCW is central to the geometric learning procedure, we present theoretical properties of it in Section 3.

We also use the DCW algorithm to compute the *data-depth* of any point in the feature space, with respect to any probability distribution function, or data cloud. A data-depth is a relative measure of how close is the given point in space to the center of a data cloud or a median of a (multivariate) probability distribution function. We discuss technical results of data-depths in the current context in Section 4 below. The crucial component of obtaining the depth of a given point with respect to a cloud of observations is to project the observations *in a single direction*, which is extremely fast and easy, apart from being an embarrassingly parallel procedure.

One immediate application of the DCW and the related data-depth algorithm is in supervised learning, presented in Section 5. Owing to the speed and efficiency of the DCW and data-depth algorithms, such classification of observations can be carried out extremely quickly, and the proposed **geometric learning** procedure may be used for *online supervised learning*. Thus, this can be adapted for a real-time analytics tool for classification in big data. Moreover, since we do not make assumptions about the geometry of the description of the data cloud $\mathbf{X}_k$ for any k, the proposed procedure is *robust* against failures of statistical assumption. Note that most statistical assumptions are essentially unverifiable declarations in high-dimensional data, hence such robustness properties are essential.

Apart from being fast and robust, the geometric learning procedure is surprisingly versatile and efficient. In the different datasets we have analysed, some of which are presented below, it seems that the proposed procedure is competitive, if not better, than standard supervised learning methods that are in popular usage. Results are presented in Section 6 for some simulated data examples, and in Section 7 for two real data examples, one of which is a high-dimensional classification problem. We conclude this paper with Section 8, where we present some caveats about using geometric learning, and some future research directions.

2 The projection quantile

We denote the open unit ball in p-dimensional Euclidean plane as $\mathcal{B}_p = \{x \in \mathbb{R}^p : ||x|| < 1\}$. The notation $||\mathbf{a}||$ stands for the Euclidean norm of a vector $\mathbf{a}$, while $\langle \mathbf{a}, \mathbf{b} \rangle$ stands for the Euclidean inner product between two vectors. For convenience, we reserve the notation $\mathbf{0}$ for a vector of zeroes, and $\mathbf{1}$ for a vector of ones, in appropriate dimensions that will be specified in the right contexts. Also, we reserve the notation $\mathbf{u}$ to denote a typical element in this open unit ball. We further reserve the notation $\mathbf{e_u}$ for the unit vector in the direction of $\mathbf{u} \in \mathcal{B}^p$. Thus, $\mathbf{e_u} = \frac{\mathbf{u}}{||\mathbf{u}||}$ when $\mathbf{u} \neq \mathbf{0} \in \mathbb{R}^p$ and $\mathbf{0}$ otherwise. For any vector $x \in \mathbb{R}^p$, we define $x_{\mathbf{u}} = \langle x, \mathbf{e_u} \rangle$. The projection of x in the direction of $\mathbf{u}$ is, $x_{\mathbf{u}}\mathbf{e_u} = ||\mathbf{u}||^{-2}\langle \mathbf{x}, \mathbf{u} \rangle \mathbf{u}$.

Let $X \in \mathbb{R}^p$ be a random variable in p-dimensional Euclidean space. For the moment, assume that the center of the distribution of X is the origin. Let, $\mathbf{q_u}$ be the $(1 + ||\mathbf{u}||)/2$-th quantile of $X_{\mathbf{u}}$, that is, $\mathbb{P}[X_{\mathbf{u}} \leq \mathbf{q_u}] = (1 + ||\mathbf{u}||)/2$. The $\mathbf{u}$-th projection quantile (PQ) is defined in

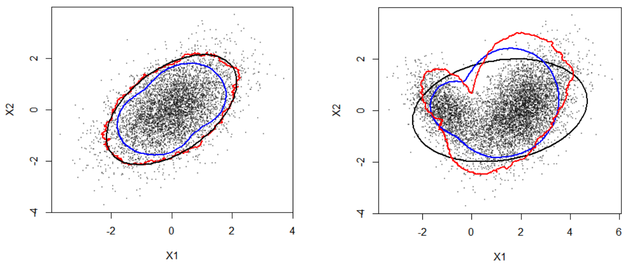

(a) (b)

Figure 1: Comparison of usual projection quantiles (blue) with weighted projection quantiles (red), along with a Gaussian confidence ellipsoid (black) for a Gaussian scatter in (a) and mixture of Gaussians in (b). Areas under the different curves are not expected to be equal.

[Mukhopadhyay and Chatterjee(2011)] as

$$Q_{proj}(\mathbf{u}) = \mathbf{q}_{\mathbf{u}}\frac{\mathbf{u}}{||\mathbf{u}||} = \mathbf{q}_{\mathbf{u}}\mathbf{e}_{\mathbf{u}}. \tag{1}$$

The *sample* version of a projection quantile, when data $\{X_1, \ldots, X_n\}$ are available, is defined exactly as above, in terms of the empirical distribution function $\mathbb{F}_n(\cdot) = n^{-1}\sum_{i=1}^{n} I_{\{X_i \leq \cdot\}}$, where I_A for any measurable set A is the indicator variable denoting whether A holds or not. Note that the data cloud $X_1, \ldots, X_n$ needs to be centered to apply the above technique. The co-ordinatewise median (the 0.5 quantile) of the data cloud acts as a good choice of the center.

The projection quantile has several interesting properties, which makes it attractive from both theoretical and algorithmic points of view. It is linearly dependent on the number of dimensions p in calculation of $X_{\mathbf{u}}$. The sample PQ computation is linear in n also. Additionally, it can be easily seen that the computation of projection quantiles in different directions are unrelated to each other, and can be trivially distributed over a network of computing cores.

We present a brief motivation of the above PQ here, by using the illustrative example of univariate and bivariate Gaussian random variables. Note that for a real random variable X, the quantile function is defined on the interval $[0, 1]$ of probabilities and has as its range as the support of the random variable, and is traditionally defined as $Q(a) = \inf\{q : \mathbb{P}[X \leq q] \geq a\}$ for any $a \in [0, 1]$. For the standard Gaussian distribution, this is illustrated in the left panel of Figure 2. Note, however, the following is also true [Ferguson(1967), Chaudhuri(1996)]:

Theorem 2.1 *The a^{th} quantile is the smallest minimizer of the function $\mathbb{E}\left[|X - q| + (2a - 1)(X - q)\right]$.*

Existence and uniqueness of $Q(a)$ is not an issue, owing to convexity of the criterion function, and hereafter we assume adequate conditions to ensure that in the *population*, the above convex criterion function has a unique minimizer. Assuming that the random variable X is absolutely continuous is sufficient for this purpose, and hereafter we assume all feature vectors are absolutely continuous random variables.

In view of the above, we may alternatively define the quantile function as being indexed by $u = 2a - 1 \in [-1, 1]$, and $Q(u)$ as the (unique) minimizer of the convex function $\mathbb{E}\left[|X - q| + u(X - q)\right]$, as illustrated by the middle panel in Figure 2. This definition of a quantile function was extended by [Chaudhuri(1996)] for p-dimensional random variables as being indexed by vectors $\mathbf{u} \in \mathcal{B}_p = \{x \in \mathbb{R}^p : ||x|| < 1\}$, and defined as minimizers $Q(\mathbf{u})$ of $\mathbb{E}\left[||X - q|| + < \mathbf{u}, X - q >\right]$, as illustrated in the right panel of Figure 2. This is a generalization of one of the earliest attempts at defining multivariate median by [Haldane(1948)]. Note that Chaudhuri's multivariate quantiles cannot be computed for $p > n$ using the algorithm given in [Chaudhuri(1996)], and requires iterative methods for even $p \leq n$. Additionally, it was seem that (a) this definition of multivariate quantiles does not capture the data geometry adequately, and (b) $Q(\mathbf{u})$ and $\mathbf{u}$ were nearly parallel in several simulated data examples. These observations motivate the projection quantile, where instead of using the full Euclidean norm of $X - q$, we only use that part of $X - q$ that is parallel to $\mathbf{u}$. Some amount of algebra reduces this procedure to the description of PQ provided above, and Figure 1 shows its efficacy.

3 The data cloud wrapper

The PQ described above does not fully capture the shape of the data geometry, mainly because of two issues. First, the spread of the data in different di-

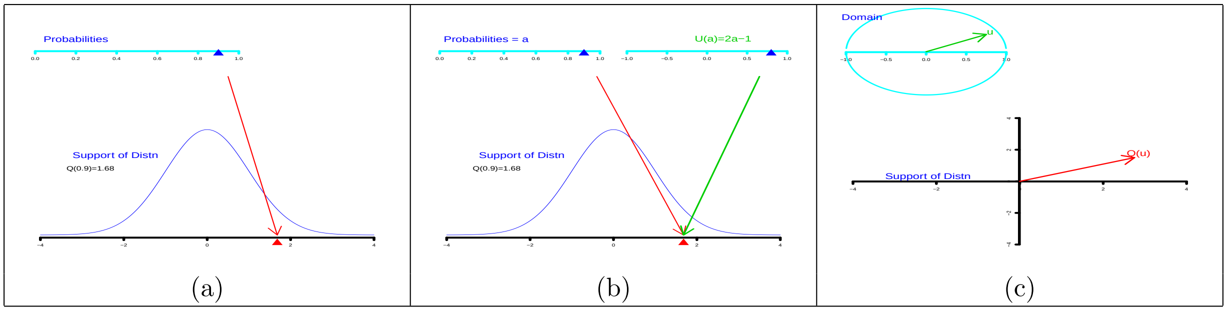

Figure 2: A graphical depiction of the quantile function in one and two dimensions

rections $\mathbf{e_u}$ from the center is different, and PQ does not accomodate for that. Second, all information related to any feature vector X_i in the directions orthogonal to $\mathbf{e_u}$ is discarded. The *data cloud wrapper* (DCW) algorithm attempts to correct these two discrepancies in the PQ, by introducing two weight functions. First, we adjust the *direction specific scaling* using $w_\mathbf{u}$ defined below. Then, we incorporate the information from the i^{th} observation in the directions orthogonal to $\mathbf{e_u}$ using another weight factor w_{2i}, also detailed below.

Recall that in accordance with the notation developed earlier, $X_{\mathbf{u}i}\mathbf{e_u}$ is the projection of X_i along $\mathbf{e_u}$. After centering (at the coordinatewise median) and scaling (using the median absolute deviation) the data, we first compute $Q_{proj}(\mathbf{u})$, the projection quantile along $\mathbf{u}$. We then compute global weights for the direction vector $\mathbf{u}$ by k-mean distance. Define d_i is the Euclidean distance of X_i from $Q_{proj}(\mathbf{u})$, and $d_{(1)} < \ldots < d_{(n)}$ are the ordered distances. We then define the k-mean distance as $\bar{d}_k = \frac{1}{n}\sum_{i=1}^{n} d_i \mathbb{I}_{\{d_i < d_{(k)}\}}$. Here, k is a tuning parameter that we choose depending on the application. We then define $w_\mathbf{u} = \exp(-a\bar{d}_k)$ as a scaling factor to be used in the direction $\mathbf{e_u}$. Our next step is to compute the norms of the vectors $||X_{\mathbf{u}\perp i}|| = ||X_i - X_{\mathbf{u}i}\mathbf{e_u}||$, which we use in the weight function $w_{2i} = \exp\left[-b\frac{||X_{\mathbf{u}\perp i}||}{||X_i||}\right]\mathbb{I}_{\{||X_{\mathbf{u}\perp i}|| \leq \epsilon\}}$. Here, b and ϵ are tuning parameters. Suppose $\{j_1, \ldots, j_{n_u}\}$ are the indices for which w_{2i} is non-zero. We now define $\tilde{X}_{\mathbf{u}j_k} = w_\mathbf{u} w_{2j_k} X_{\mathbf{u}j_k}$, for $k = 1, \ldots, n_u$. The DCW in the direction $\mathbf{e_u}$ is obtained by selecting the $\alpha = (1 + ||\mathbf{u}||)/2$-th quantile of $\tilde{X}_{\mathbf{u}j_1}, \ldots, \tilde{X}_{\mathbf{u}j_{n_u}}$. Let it be $\tilde{q}_\mathbf{u}$. The DCW is the direction $\mathbf{e_u}$ is defined as $\tilde{Q}_{proj}(\mathbf{u}) = \tilde{q}_\mathbf{u}\mathbf{e_u}$.

In order to state the theoretical properties of the DCW, first define $\tilde{X}_{\mathbf{u}i} = w_\mathbf{u} w_{2j_k} X_{\mathbf{u}i}$, for $i = 1, \ldots, n$. Also, consider the following two functions

$$\Psi_\mathbf{u}(X, q) \quad = \quad \mathbb{I}_{\{||X_{\mathbf{u}\perp i}|| \leq \epsilon\}}\left[|\tilde{X}_{\mathbf{u}i} - q| + ||\mathbf{u}||(\tilde{X}_{\mathbf{u}i} - q)\right],$$

$$g_\mathbf{u}(X, q) \quad = \quad \mathbb{I}_{\{||X_{\mathbf{u}\perp i}|| \leq \epsilon\}}\left[\left(2\mathbb{I}_{\{\tilde{X}_{\mathbf{u}i} \leq q\}} - 1\right) - ||\mathbf{u}||\right].$$

Our results are based on the *population level* properties of the functions $\Psi_\mathbf{u}(X, q)$ and $g_\mathbf{u}(X, q)$, that is, their behavior when we take an expectation of these functions with respect to the measure extended by X. Such properties are not assumed for sample level functions. An extremely easy example where population and sample values differ may be seen in the context of a Binomial (n, θ) random variable Z. Note that the expectation of Z/n is θ, which is a smooth function on $(0, 1)$. However, the sample expectation, ie, the same functional computed under the empirical distribution function, is just Z/n, which is supported only on discretely many values, and is not a smooth function.

We assume that $\mathbb{E}\Psi_\mathbf{u}(X, q)$ is finite for all potential choices of q, and has a unique minimizer, which we call $q^*_\mathbf{u}$. This merely states that there is a unique population parameter to estimate. The sample version does not require uniqueness, but that may be enforced, as is traditionally done, by defining the minimizer to be the infimum over all possible values at which the minimum is reached. In this framework, we have the following results:

Theorem 3.1 *The sample DCW is a consistent estimator of the population DCW, that is $q_\mathbf{u} \to q^*_\mathbf{u}$ almost surely as sample size $n \to \infty$.*

Theorem 3.2 *Under the additional* **population level** *conditions that $\mathbb{E}g^2_\mathbf{u}(X, q^*_\mathbf{u}) < \infty$, and that the function $\mathbb{E}\Psi_\mathbf{u}(X, q)$ is twice continuously differentiable at $q^*_\mathbf{u}$ with the second derivative H being positive definite, then as $n \to \infty$*

$$n^{1/2}(q_\mathbf{u} - q^*_\mathbf{u}) = -n^{-1/2}H^{-1}S_n + o_P(1),$$

where $S_n = \sum_{i=1}^{n} g_\mathbf{u}(X_i, q^*_\mathbf{u})$. This implies, in particular, that $n^{1/2}(q^*_\mathbf{u} - q^*_\mathbf{u})$ is asymptotically Normal, with asymptotic variance $H^{-1}VH^{-1}$ where $V = \mathcal{V}ar\ g_\mathbf{u}(X, q^*_\mathbf{u})$.

The proofs of these results, and other theorems that follow, require considerable mathematical details. We present a very brief sketch of the main line of argument in the supplementary material, and the details can be made available as needed.

4 Data depth using the DCW

We consider the support of the feature vector, $\mathcal{X}$ to be a convex set in $\mathbb{R}^p$. For any given point $\mathbf{p} \in \mathcal{X} \setminus \{\mathbf{0}\}$ the support of a feature of an absolutely continuous random vector X with cumulative distribution function F, we define the *data-depth* as $D(\mathbf{p}, F) = \exp(-\alpha_{\mathbf{p}})$, where $\mathbf{u} = \alpha_{\mathbf{p}}\mathbf{p}/||\mathbf{p}||$, and $\tilde{Q}_{proj}(\mathbf{u}) = \mathbf{p}$. We extend this to the point $\mathbf{p} = \mathbf{0}$ by defining $D(\mathbf{0}, F) = 1$. This essentially means that $\alpha_{\mathbf{p}} \in (0, 1]$ is the norm of $\mathbf{u}$, which has the same direction as $\mathbf{p}$, such that $\mathbf{u}^{th}$ DCW is exactly $\mathbf{p}$.

The following properties are available for the data depth function $D(\mathbf{p}, F)$:

Theorem 4.1 *1. $D(\mathbf{p}, F) = 1$ if and only if $\mathbf{p} = \mathbf{0}$.*

2. $D(t\mathbf{p}, F) \leq D(\mathbf{p}, F)$ for all $\mathbf{p} \in \mathcal{X}$, and all $t \in [0, 1]$.

3. The directional derivative of $D(\mathbf{p}, F)$ with respect to $\mathbf{p}$ exists.

4. The depth function $D(\mathbf{p}, F)$ is smooth in te second argument, in the sense that the Gateux derivative exists.

5. $D(\mathbf{p}, F) \to 0$ as $||\mathbf{p}|| \to \infty$.

Note that the first two properties are the essential properties of a data-depth, while the rest of the results are technical properties that help understand the depth function better.

5 Geometric classification technique

One immediate application of the DCW and the related data-depth algorithm is in supervised learning. Consider a feature vector $X \in \mathcal{X} \subseteq \mathbb{R}^p$ for some (potentially high) dimension p, associated with a label $Y \in \mathcal{Y} = \{0, 1, \ldots, K-1\}$. Assumed that the observed data is a random sample $\{(X_i, Y_i) \in \mathcal{X} \times \mathcal{Y} \subseteq \mathbb{R}^p \times \{0, 1, \ldots, K-1\}\}$ of such (X, Y) pairs. Here K, the total number of labels, is assumed known. Without loss of generality, we assume that observations indexed by $S_k = \{i_{k1}, \ldots, i_{kn_k}\}$ share the common label $Y_{i_{kj}} = k$, for any $k \in \mathcal{Y} = \{0, \ldots, K-1\}$. We assume that $\cup_{k=0}^{K-1} S_k = \{1, \ldots, n\}$, and $S_k \cap S_{\tilde{k}} = \varnothing$ whenever $k \neq \tilde{k}$. We denote the n_k feature observations corresponding to S_k by $\mathbf{X}_k = (X_{i_{k1}}, \ldots, X_{i_{kn_k}})$.

We elicit the label of any new or unlabeled feature vector $x \in \mathcal{X}$ by computing its depths with respect to the K different data clouds of observations $\mathbf{X}_k = (X_{i_{k1}}, \ldots, X_{i_{kn_k}})$. We may then choose the label that corresponds to the highest depth value, or construct labels using more complex usage of the K depth values obtained for x. For example, one alternative to simply choosing the highest-depth label would be to not classify an unlabeled observation if the maximum depth is below a threshold, thus paving the way for potentially extending this algorithm to unsupervised and semi-supervised classification problems, which we do not pursue here.

Notice that the geometric learning-based separating boundary between two labeled classes in the feature space is essentially the locus of the points where the data-depths are equal from both the classes. Thus, the separating curves between labeled classes are essentially *isodepth curves*. This notion can be extended to multiple labeled classes easily, and is of independent interest.

Nevertheless, note that in order to classify a new or unlabeled observation, it is not necessary to obtain the entire isodepth curves. The only computation that needs to be performed is to obtain the data-depth *in the direction of the unlabeled observation* relative to each labeled class, which is trivially a parallelizable procedure requiring at most n one-dimensional projections and few other simple computations. This leads to the geometric learning algorithm being very much amenable to active learning as well as online learning of class labels.

It may be noted that existing techniques for supervised learning either impose shape restrictions explicitly or tacitly, or suffer from curse of dimensionality, or are slow, sequential procedures requiring multiple passes through the data. Many methods of supervised learning suffer from multiple of these issues. For example, methods like logistic regression for two or more class labels, as well as linear or quadratic discriminant analysis explicitly make parametric statistical assumptions, which imply strong restrictions on the shape of the allowed data layout. The classical version of these algorithms are inapplicable for data in high dimensions, and require additional assumptions, typically of sparsity of some functional of the feature vector distributions, for usability in big data. Some of these additional assumptions are unverifiable in data. Nearest neighbor rules implicitly make similar assumptions with a choice of metric and tuning parameters, while support vector machines make an implicit choice of allowable geometry using the kernel function. Methods like (multivariate) density estimation and subsequent learning procedures suffer from the curse of dimensionality. Decision trees and ensemble-based methods like classification and regression trees, bagging, random decision forests, boosting require iterative and often sequential computation, and may impose shape restrictions on the data and may suffer from curse of dimensionality depending on the algorithmic details.

6 Geometric learning example: simulated data

In this section we use two simulated datasets to demonstrate the key characteristics of the proposed geometry learning algorithm, and compare its performance with state-of-the-art alternatives.

The simulated data contains two classes, and is depicted in Figure 3 with black and red points. We present the two simulated datasets in this figure, in the two panels. In both panels, the black points are clustered in the apple shaped figure, while the red points are in the top leaf cluster. The dotted lines in green and black are the DCW curves corresponding to the black and red observations respectively, corresponding to $||\mathbf{u}|| = 0.9$. The solid blue curve indicates the iso-depth curve for this dataset, which acts as the curve of separation for the two groups of data. In order to evaluate the classification accuracy and speed of our algorithm, we randomly selected 80% of the observations from each group for training, and evaluated the geometric learning algorithm on the rest 20% test data from each group. For comparison purposes, we also used several standard classification algorithms on identical training and testing datasets. This process was repeated 1000 times to ensure sufficient randomization. The running time are based on running each of the methods on a 1 GHz, quadruple core computer in R 3.1.1 platform. We present the classification accuracy results in Table 1.

As can be seen from Table 1, the geometric learning algorithm is comparable or better in terms of classification accuracy and speed compared to the state-of-the-art methods. In fact, it is considerably fast in comparison to the other algorithms which achieve similar levels of accuracy in different datasets, of which we have chosen two illustrative examples. In particular, the geometric learning technique is considerably faster than random forest and support vector machines (SVM), and slightly faster than the k-nearest neighbor (KNN) algorithm. In general, parametric methods like linear or quadratic discriminant analysis (LDA, QDA), and logistic regression, or procedures like neural networks do not achieve a good class separator, especially in dataset (b) where the classes are not as distinct as in case of dataset (a).

We used the standard packages and routines in the open source software `R`, namely `glm, lda (MASS), qda (MASS), randomForest, svm (e1071), nnet, knn (class)` for the existing supervised learning methods reported here. In the random forest procedure, the number of trees for each run was kept at 500, sampling was done with replacement, and the rest of the parameters were run with default setting. Radial basis kernel $(= \exp(-\gamma|u - v|^2))$ was used for the SVM fit of type *C-Classification* using a scaling of 1 and a class weight equal to the proportion of observation in each class in the train set. For neural nets, the size of the hidden layer was set at 2, case-wise sample weights were set at 1, and entropy fit was used. More details on the classification techniques used for our analysis, and detailed graphical results from this simulation study may found in the supplementary material. Algorithmic and statistical details of these learning techniques can be found in [Hastie, T. and R. Tibshirani and J. Friedman(2009)].

7 Performance of the Algorithm on Standard Datasets

We show the performance of the dataset on two multiclass multivariate datasets, namely the celebrated Fisher's iris dataset, and the colon dataset from the `R` package `cepp`.

7.1 Fisher's Iris Dataset

This is perhaps the best known dataset to be found in the pattern recognition, learning and statistical classification literature. Performance on this dataset is a litmus test for any new proposed machine learning method. The data contains three classes of Iris plants of 50 instances each. The three classes are *Iris setosa*, *Iris versicolor* and *Iris virginica.* There are four features related to the Iris plant and flower in this dataset: sepal length, sepal width, petal length and petal width, all in centimeters. We use the same methods and techniques as in the simulated data

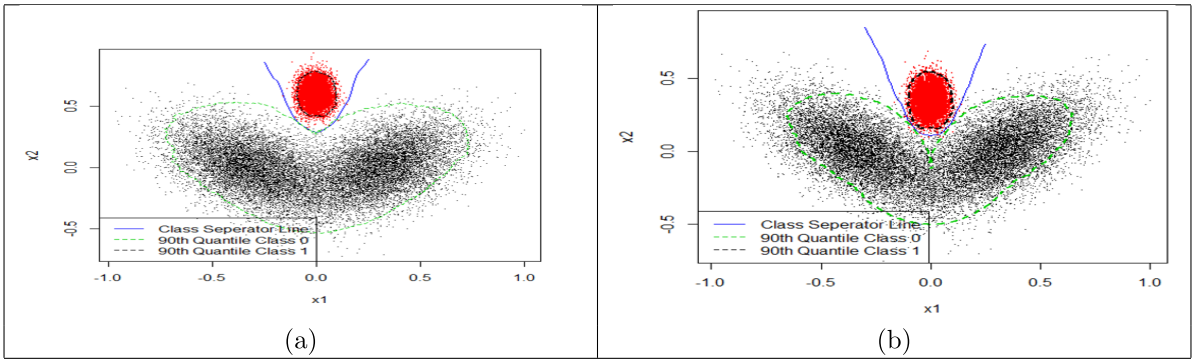

(a)

(b)

Figure 3: Isodepth separation curves for a binary classification problem in two datasets

analysis discussed above.

In Table 2 we present the average classification accuracy in the test data sets from the Iris data. The running time of all the algorithms are very similar since the dataset is small with 150 observations and 4 predictors. In terms of performance, while all methods perform well, the proposed Geometric Learning algorithm is the second best, beaten only marginally by the k-nearest neighbor method.

7.2 Classifying big data: the colon cancer dataset

The colon dataset is a publicly available dataset for $n = 62$ individuals related to colon cancer. This dataset was generated using Affymetrix oligonucleotide arrays, and contains expressions levels for 40 tumor and 22 normal colon tissues. Out of the originally measured 6500 human genes, $p = 2000$ with the highest minimal intensity across the tissues are selected for classification purposes. Each score represents a gene intensity derived in a process described in [Alon, A., *et. al*(1999)]. Note that in this case dimension p is considerably higher than sample size n, and thus represents a big data supervised learning problem.

It can be seen that the Geometric Learning Algorithm is the most successful among the supervised learning methodologies that were usable for this dataset, both in terms of prediction accuracy, as well as n terms of speed. Methods not reported here were not applicable without additional unverifiable technical assumptions. Support vector machines perform marginally better in terms of accuracy, but requires an 80-fold increase in computing time. The k-nearest neighbor method has comparable accuracy to Geometric Learning, but requires nearly 7-fold more run time for each single choice of k, and the performance is dependent on the choice of k. For example, we ran the k-nearest neighbor algorithm for $k = \{1, \ldots, 15\}$, to obtain the best performance of this method, consequently the actual process time should be multiplied by 15, and is thus about a 100-fold more than Geometric Learning. Figure 4 shows the dependence of KNN on different values of k.

8 Conclusions and future directions

The geometric learning algorithm can be seen to be very versatile, and applicable in complicated supervised learning problems, as well as in high dimensions. One future research to pursue is on theoretical quantification of its classification error bound. Another important consideration in this line of research is to evaluate its performance in unsupervised learning problems.

Some of the limitations of the geometric learning method arise from the topological restrictions it imposes on the data corresponding to any labeled class. While such restrictions are minimal, it is nevertheless unlikely to succeed in classification problems where the data cloud for any class consists of more than one connected component, or have genus greater than zero. We can envisage how to extend the geometric learning algorithm to address these kind of data features, but nevertheless additional research needs to be carried out.

References

[Alon, A., *et. al*(1999)] Alon, A., *et. al.* Broad Patterns of Gene Expression Revealed by Clustering Analysis of Tumor and Normal Colon Tissues Probed by Oligonucleotide Arrays. *Proc. Natl. Acad. Sci. USA*, 96:6745–6750, 1999.

[Chaudhuri(1996)] P. Chaudhuri. On a geometric notion of quantiles for multivariate data. *J. of Amer. Stat. Assoc.*, 91:862–872, 1996.

[Ferguson(1967)] T. Ferguson. *Mathematical Statistics, A Decision Theoretic Approach.* Academic Press, New York, NY, 1967.

[Haldane(1948)] J. Haldane. Note on the median of a multivariate distribution. *Biometrika*, 35:414–415, 1948.

[Hastie, T. and R. Tibshirani and J. Friedman(2009)] Hastie, T. and R. Tibshirani and J. Friedman. *The Elements of Statistical Learning: Data Mining, Inference, and Prediction.* Springer, 2009.

[Mukhopadhyay and Chatterjee(2011)] N. Mukhopadhyay and S. Chatterjee. High dimensional data analysis using multivariate generalized spatial quantiles. *J. Mult. Anal.*, 102-4:768–780, 2011.

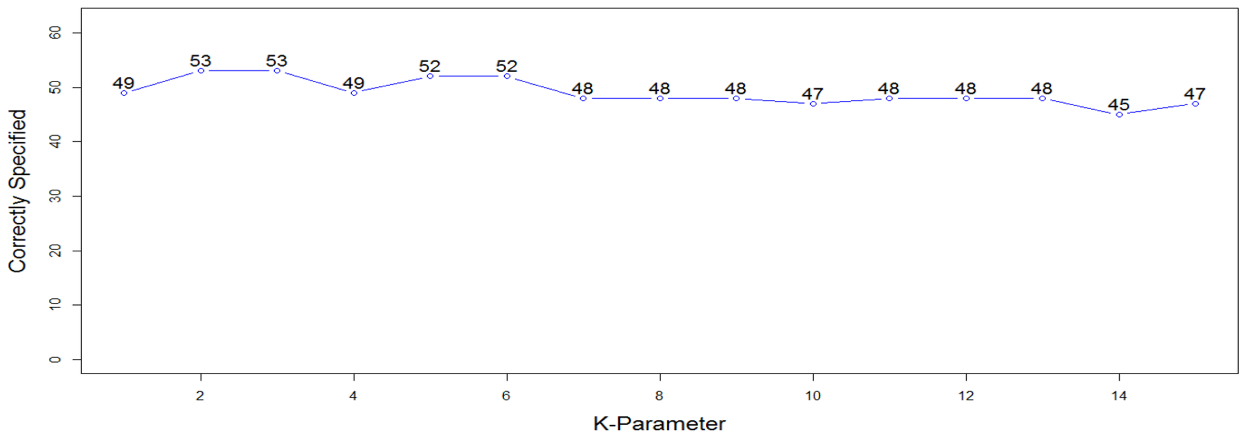

Figure 4: Correct classification (out of 62 cases) for KNN as a function of the choice of k in colon cancer data

	Data (a)		Data (b)	
Method	Accuracy	Run time	Accuracy	Run time
Geometric learning	0.996	1.46	0.976	1.48
Logistic regression	0.981	0.28	0.901	0.31
LDA	0.969	0.22	0.881	0.20
QDA	0.992	0.27	0.974	0.21
Random forest (500 trees)	0.998	23.61	0.976	31.77
Neural network	0.967	4.76	0.962	3.56
SVM	0.984	6.45	0.974	8.54
KNN	0.997	1.53	0.989	1.62

Table 1: Comparison of several supervised learning algorithms on the simulated example, in randomly selected test sets. The classification accuracy is the average proportion of test sets observations correctly classified.

Method	Accuracy
Geometric learning	0.9733
LDA	0.9600
QDA	0.9667
Random forest (500 trees)	0.9667
Neural network	0.9267
SVM	0.9533
KNN	0.9741

Table 2: Performance of different classification algorithms on the Fisher iris dataset

Method	# Mis-classified	Accuracy	Run time
Geometric Learning	9	0.854	0.21
Random forest (500 trees)	10	0.839	226.92
LDA	15	0.758	45.12
SVM	8	0.871	17.36
KNN(K=3)	9	0.854	1.41

Table 3: Classification results in the colon cancer data